



Article

Safe and Scalable Polyethylene Glycol-Assisted Hydrothermal Synthesis and Laser Cooling of 10%Yb³⁺:LiLuF₄ Crystals

Elena A. Dobretsova ^{1,2} , Anupum Pant ^{1,3}, Xiaojing Xia ⁴, Rachel E. Gariepy ¹ and Peter J. Pauzauskie ^{1,5,*} 

¹ Department of Materials Science & Engineering, University of Washington, Seattle, WA 98195, USA; elenadobretsova89@gmail.com (E.A.D.); anupum.pant@gmail.com (A.P.); rachelg2@uw.edu (R.E.G.)

² Prokhorov General Physics Institute of the Russian Academy of Sciences, 119991 Moscow, Russia

³ Intel Corporation, Hillsboro, OR 97124, USA

⁴ Molecular Engineering and Science Institute, University of Washington, Seattle, WA 98195, USA; xiaxj@uw.edu

⁵ Physical Sciences Division, Physical and Computational Sciences Directorate, Pacific Northwest National Laboratory, Richland, WA 99352, USA

* Correspondence: peterpz@uw.edu; Tel.: +1-(206)-543-2303

Featured Application: A safe and scalable method is reported for the synthesis of rare earth doped lithium fluorides that allows for much larger bulk syntheses of these materials that would be challenging when using more hazardous reagents.

Abstract: Rare earth doped lithium fluorides are a class of materials with a wide variety of optical applications, but the hazardous reagents used in their synthesis often restrict the amount of product that can be created at one time. In this work, 10%Yb³⁺:LiLuF₄ (Yb:LLF) crystals have been synthesized through a safe and scalable polyethylene glycol (PEG)-assisted hydrothermal method. A combination of X-ray diffraction (XRD) analysis, scanning electron microscopy (SEM), and photoluminescence (PL) measurements were used to characterize the obtained materials. The influence of reaction temperature, time, fluoride source, and precursor amount on the shape and size of the Yb:LLF crystals are also discussed. Calibrated PL spectra of Yb³⁺ ions show laser cooling to more than 15 K below room temperature in air and 5 K in deionized water under 1020 nm diode laser excitation measured at a laser power of 50 mW.

Keywords: laser refrigeration; hydrothermal synthesis; crystal growth; ratiometric thermometry



Citation: Dobretsova, E.A.; Pant, A.; Xia, X.; Gariepy, R.E.; Pauzauskie, P.J. Safe and Scalable Polyethylene Glycol-Assisted Hydrothermal Synthesis and Laser Cooling of 10%Yb³⁺:LiLuF₄ Crystals. *Appl. Sci.* **2022**, *12*, 774. <https://doi.org/10.3390/app12020774>

Academic Editor: Galina Nemova

Received: 27 November 2021

Accepted: 8 January 2022

Published: 13 January 2022

Publisher's Note: MDPI stays neutral with regard to jurisdictional claims in published maps and institutional affiliations.



Copyright: © 2022 by the authors. Licensee MDPI, Basel, Switzerland. This article is an open access article distributed under the terms and conditions of the Creative Commons Attribution (CC BY) license (<https://creativecommons.org/licenses/by/4.0/>).

1. Introduction

Rare earth lithium fluorides (RELiF₄) with a scheelite structure are widely used in various fields such as theranostics [1], long-term in vivo bioimaging [2,3], photothermal therapy [4–6], ratiometric temperature sensing [7], transparent volumetric displays [8,9], multi-level anti-counterfeiting applications [10], photocatalysis [11], photovoltaics [12], scintillating materials [13], and refrigeration through laser radiation [14–20]. These materials also show promise for solid-state laser applications [21].

Recently, it has been demonstrated that low-cost, low-temperature hydrothermal processing can be used to grow YLiF₄ [17], NaYF₄ [22], KLuF₄ [23], and LiLuF₄ [24] crystals that are capable of solid-state laser refrigeration. However, the use of ammonium bifluoride inhibits the production of large amounts of these materials due to the danger of hydrofluoric acid formation in solution, which can then form gaseous hydrogen fluoride during the autoclave portion of the synthesis. Using polyethylene glycol (PEG) in place of NH₄HF₂ helps improve the solubility of lithium ions while also reducing potential hazards posed by the use of ammonium bifluoride and, as a result, makes this method safer and more scalable.

Due to the complexity of hydrothermal systems, various internal and external factors can fundamentally affect the purity, crystal structure, morphology, and physical properties of the obtained materials. For example, it has been shown that LiOH concentration is the key factor responsible for the shape evolution and phase control of RELiF_4 nanocrystals at selected temperatures [25]. It has also been shown that the use of EDTA as a chelating agent in the reaction is essential to obtain highly crystalline and smooth $\text{Er}^{3+}:\text{LiYbF}_4$ microparticles [26]. Most importantly, these hydrothermal materials show more efficient luminescence with further heat treatment. Higher reaction temperatures and prolonged reaction times have been shown to facilitate the formation of more stable LiYbF_4 microcrystals [27]. The substitution of Li^+ in $\text{Na}_{(1-x)}\text{Li}_x\text{ReF}_4$ not only causes a phase transition but also induces variation in the morphology, size, and luminescent properties of the final microcrystals [28]. Taking these observations into consideration, parameters other than the fluoride source, such as temperature, precursor amount, and reaction length, must be carefully controlled and examined to determine their effect on the final crystal.

In this work, we report a method for PEG-assisted hydrothermal synthesis of Yb^{3+} -doped lithium lutetium fluoride ($\text{Yb}:\text{LLF}$) microcrystals and discuss the influence of various factors on the growth of the $\text{Yb}:\text{LLF}$ microcrystals and their ability to undergo laser refrigeration.

2. Materials and Methods

Synthesis of $10\% \text{Yb}^{3+}:\text{LiLuF}_4$. The reagents used in this synthesis are identical to those used in a similar synthesis in previous work [24].

The following synthesis (Figure 1) is a slight modification of previous work [17]. In contrast to the referenced procedure, yttrium nitrate ($\text{Lu}(\text{NO}_3)_3$) and ytterbium nitrate ($\text{Yb}(\text{NO}_3)_3$) of 99.999% purity were used as purchased from Sigma-Aldrich. The nitrate powders were dissolved in Millipore deionized (DI) water to achieve a stock concentration of the respective nitrates. Additionally, nitric acid (HNO_3) and ammonium bifluoride (NH_4HF_2) were not used in this synthesis. Lithium fluoride (LiF) and polyethylene glycol (PEG, $M_n = 4000$) were used directly without any purification. For this synthesis, 28.8 mL of 0.5 M $\text{Lu}(\text{NO}_3)_3$ and 3.2 mL of 0.5 M $\text{Yb}(\text{NO}_3)_3$ were mixed with 16 mmol of EDTA and 30 mmol of LiOH in 20 mL of Millipore DI water at 50 °C while stirring for 30 min to form solution A. Subsequently, 64 mmol of LiF were dissolved in 30 mL of 10 wt.% PEG Millipore DI water solution at room temperature while stirring for 1 h to form solution B. Solutions A and B were mixed together while stirring for 30 min to form a homogeneous white suspension, which was transferred to a 2-L Teflon-lined autoclave and heated to 180 °C for 24 h. After the autoclave cooled to room temperature, the $\text{Yb}:\text{LLF}$ particles were recovered by centrifuging and washing with ethanol and Millipore DI water three times. The final white powder was obtained by calcining at 300 °C for 2 h in air, which was determined to be the ideal temperature for calcination via XRD and SEM (Figures S1 and S2). The theoretical yield was 4.120 g of $\text{Yb}:\text{LLF}$. The actual yield was 2.0 g, for a yield percentage of 48.5%

Multiple variations of this base synthesis were performed to examine the effects of different variables on the crystals. In some experiments, the reagent amounts were reduced by a factor of 4. Other syntheses were performed at temperatures other than 180 °C, including 100, 120, 130, 200, and 220 °C for 24 h. The effect of time on the synthesis was also examined, with data from some syntheses collected at 3 h, 5 h, and 14 h, as well as the standard 24 h time point.

Characterization. Scanning electron microscopy (SEM) images were taken on an FEI Sirion XL30 SEM at an accelerating voltage of 15 keV. Powder X-ray diffraction (XRD) patterns were obtained on the Bruker F8 Focus Powder XRD with $\text{Cu K}\alpha$ (40 kV, 40 mA) irradiation ($\lambda = 0.154$ nm). The 2θ angle of the XRD data was 16° to 93°, and the scanning rate was 0.36° s^{-1} . PL spectra were registered following a method outlined in previous work [24].

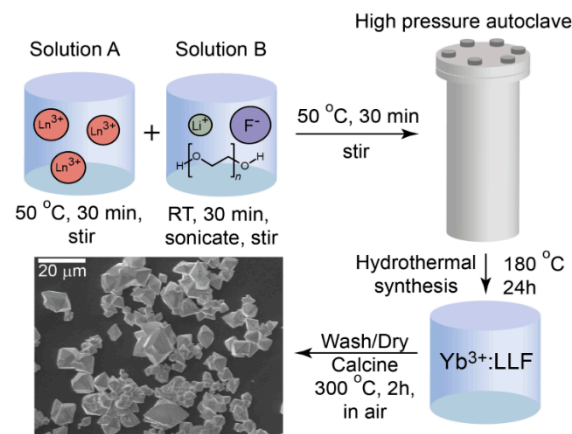


Figure 1. Schematic of the base PEG-assisted hydrothermal synthesis of Yb:LLF microcrystals.

When collecting photoluminescence spectra, Yb:LLF crystals were attached to optical fibers for the sake of thermal isolation. The crystals were then optically excited in air using a 1020 nm diode laser with irradiances ranging from 0.08 to 1 MW/cm². Temperatures were calibrated for individual Yb:LLF grains using an optical cryostat. Temperatures were scanned from 300 to 400 K with a low laser irradiance of 0.04 MW/cm² to minimize any photothermal effects caused by optical excitation. Cold Brownian motion data were collected using a home-built optical trapping setup and following a procedure from previous work [17].

3. Results

Scanning electron microscopy (SEM) of two different Yb:LLF crystals are shown in Figure 2a. In the first case (Figure 2a), the Yb:LLF crystals have been synthesized through an NH₄HF₂-assisted hydrothermal method [17,24]. They have a tetragonal bipyramidal morphology with a dominating (101) surface. The Yb:LLF crystals synthesized through the PEG-assisted hydrothermal method (Figure 2b) have two dominating surfaces: (101) and (112), respectively, which was predicted in Littleford's works [29,30] for a yttrium lithium fluoride (YLF) crystal. Figure S3 also shows the room-temperature FTIR spectra of the Yb:LLF crystals obtained at different conditions. The weak peaks in the FTIR spectra can be attributed to atmospheric water and carbon dioxide adsorbed on the optical elements of the spectrometer and on the samples, and the absence of strong bands in the range of 1000–4000 cm⁻¹ implies that there is no residual PEG and minimal oxyfluorides on the surface of the crystals regardless of synthesis method.

X-ray diffraction analysis confirms that crystals from both syntheses adopt a tetragonal scheelite structure (ICDD number 04-002-3255) with space group *I*4₁/*a* (Figure 2c). Comparison of the two X-ray diffraction spectra of Yb:LLF (Figure 2c) corresponding to NH₄HF₂- (blue) and PEG-assisted (red) syntheses gives different ratios of *I*(101):*I*(112), which correlates with the morphology of the Yb:LLF crystals. Stereographic projections of crystal facets related to the most intensive XRD peaks are shown in Figure 2d (inset) as red circles.

Crystals grown using the base PEG-assisted synthesis described previously were subjected to photoluminescence (PL) measurements to examine the cooling abilities of the crystals grown via this new method. Crystals grown via the base synthesis method were used due to the method's ability to consistently produce pure single crystals with only one phase. This avoids issues caused by parasitic energy transfer or luminescence quenching due to impurities, maximizing the laser cooling power of the crystals. The PL spectra obtained at different 1020 nm laser powers are shown in Figure 3a. Changes in the ratio of the integrated emission bands *R*₁ and *R*₂ (and their respective intensities in a.u., *I*₁, and *I*₂), which stem from transitions between energy states *E*₆-*E*₁ and *E*₅-*E*_{2,3}, respectively, are directly correlated to a change in the crystal temperature through a Boltzmann distribution

(Figure 3b). Ratiometric spectral measurements were used to calibrate temperature in which $\ln(I_1/I_2)$ varies linearly with $1/T$ (calibration shown in Figure S4). The decrease in the logarithmic ratio of I_1 to I_2 with increasing irradiance reflects a decrease in the internal lattice temperature of approximately 15 K below room temperature (Figure 3b). Analogous laser cooling trends (approximately 5 K below room temperature) were observed for individual Yb:LLF grains optically trapped in water (Figure 3c). These values are comparable to cooling temperatures Yb:LLF crystals obtained via the NH_4HF_2 -assisted synthesis. [24] Additionally, these crystals exhibit much greater cooling capability than 5%-Yb doped LLF crystals grown via the Czochralski process but do not cool to the cryogenic temperatures reached by Czochralski-grown Yb:YLF crystals [15,31].

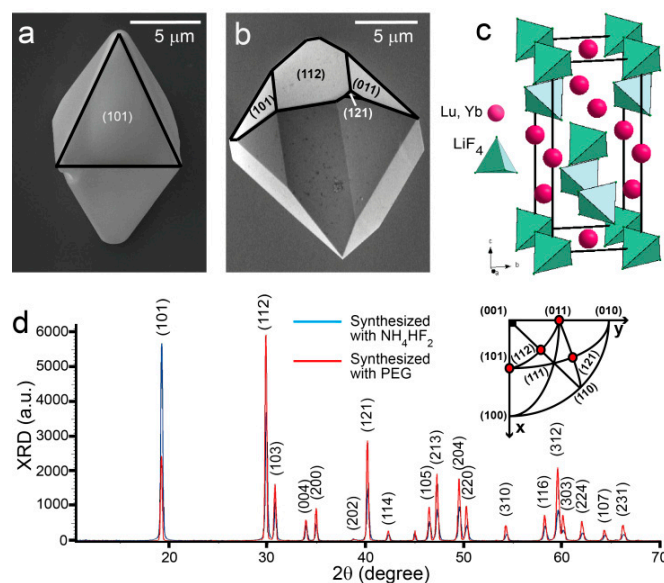


Figure 2. Characterization of Yb:LLF crystals. Scanning electron microscope images of faceted Yb:LLF particles synthesized with NH_4HF_2 - (a) and PEG-assisted (b) hydrothermal syntheses. Scale bar = 5 μm . Types of facets are indicated in parentheses. (c) Schematic of a Scheelite crystal structure of Yb:LLF with $I4_1/a$ space group symmetry. (d) Powder XRD pattern of Yb:LLF crystals following NH_4HF_2 - (blue) and PEG-assisted (red) hydrothermal synthesis, indicating a Scheelite crystal structure. Inset: stereographic projections of crystal facets related to the most intensive XRD peaks.

Reducing the concentration of reagents by a factor of four leads to the synthesis of significantly smaller crystals. The low concentration synthesis produced crystals around 5 μm in size, whereas the standard synthesis could produce crystals as large as 20 μm . Although their size is greatly changed, the morphology of the crystals remains the same regardless of the reagent concentration. The (112) plane remains clearly visible on both sets of crystals (Figure S5).

XRD data from a range of experimental temperatures spanning from 100 $^\circ\text{C}$ to 200 $^\circ\text{C}$ are shown in Figure 4. At lower temperatures, a variety of side products can be seen in the XRD data, including LuF_3 and LiLuO_2 . Unreacted or undissolved LiF can also be seen in many of the XRD patterns. A stable, single phase of Yb:LLF is not reached after 24 h unless the standard reaction temperature of 180 $^\circ\text{C}$ or above is used. Additionally, the size of the formed crystals also increases with reaction temperature, which can be seen in SEM images (Figure S6). Reaction time also plays a factor in the generation of a single, stable Yb:LLF phase. At lower time points, the XRD data shows mostly unreacted LiF and little to no evidence of the Yb:LLF crystals. After 14 h, a significant Yb:LLF phase can be seen, and only traces of LiF remain (Figure S7). SEM also shows that increasing the length of the synthesis causes the crystal facets and morphology to be more well-defined and fully formed (Figure S8).

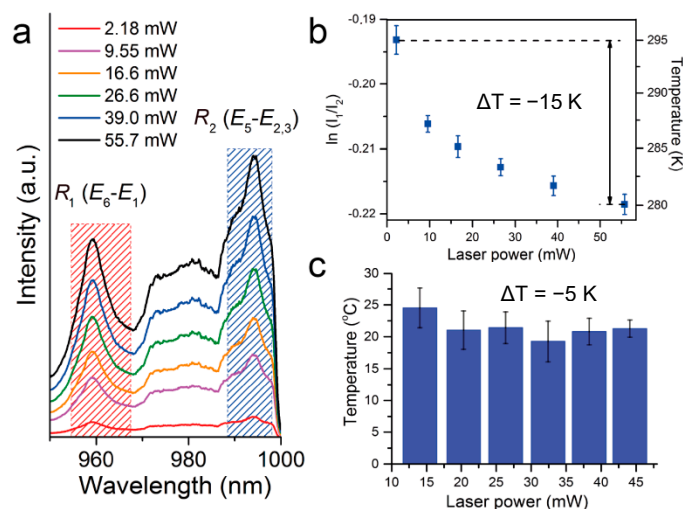


Figure 3. Laser cooling of Yb:LLF crystals. (a) PL spectra of the Yb:LLF crystal on a SiO₂ optical fiber in air under 1020 nm diode laser excitation measured at different irradiances. (b) Cryostat calibration of PL spectra of the Yb:LLF crystal on a SiO₂ optical fiber in air under 1020 nm diode laser excitation measured at different irradiances. (c) Laser refrigeration of the Yb:LLF crystal in deionized water measured via cold Brownian motion analysis at different irradiances.

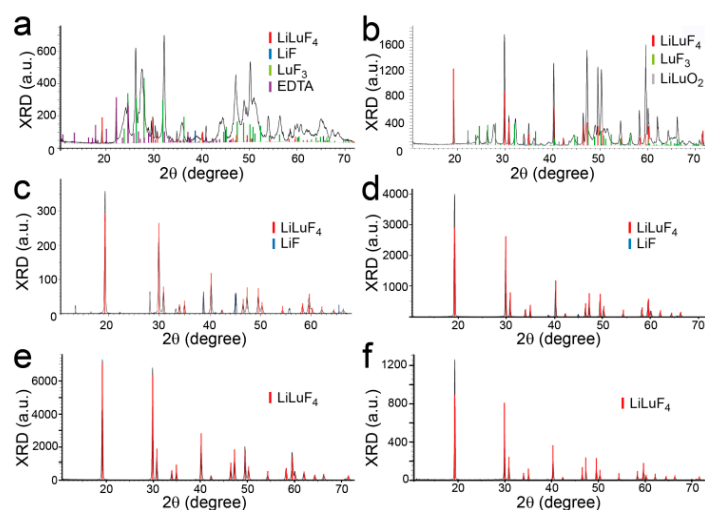


Figure 4. Powder XRD pattern of crystals following PEG-assisted hydrothermal synthesis at: (a) 100 °C, (b) 120 °C, (c) 130 °C, (d) 150 °C, (e) 180 °C, and (f) 200 °C, for 24 h.

4. Discussion

The fluoride source and inclusion of PEG clearly affect the morphology of the Yb:LLF crystals. The (112) planes seen in all crystals synthesized via the PEG-assisted method indicate that the PEG lowers the surface energy of that plane, changing the Wulff construction of the crystal and allowing it to form during the hydrothermal synthesis. In spite of this additional plane, the stoichiometric 1:1:4 product is formed, as confirmed by XRD. This is of particular interest as other RELiF₄ materials, such as NaYF₄, do not form a stoichiometric phase. [32] Additionally, this extra plane does not impact the crystals' cooling abilities, which are comparable to those shown by crystals formed using the ammonium bifluoride synthesis. It can then be concluded that this synthesis method is not only effective, but a safe and scalable alternative to the ammonium bifluoride synthesis when attempting to synthesize large amounts of Yb:LLF crystals. This synthesis generates high amounts of

product while avoiding the hazards of hydrofluoric acid formation and hydrogen fluoride gas generation.

Compared to the fluoride source, the temperature and length of the reaction do not significantly impact crystal morphology but, instead, are key factors in forming a pure and highly crystalline Yb:LLF phase, as well as impacting the size of the crystals formed. The number of precursors remaining in solution at shorter time points, specifically undissolved or unreacted LiF, could be eliminated by allowing the reaction to proceed for longer times, further improving the yield of the reaction. The size of the crystals can also be controlled by the concentration of precursors in an aqueous solution. By combining the size control demonstrated by changing the reaction temperature and the size control demonstrated by the precursor concentrations, it could be possible to finely control the size of the crystals.

5. Conclusions

Yb:LLF crystals with a scheelite structure (space group $I4_1/a$) have been synthesized through a safe and scalable PEG-assisted hydrothermal approach. We show that size and morphology can be finely controlled by changing reaction conditions such as temperature, time, fluoride source, and precursor amount. The results show that higher temperature and prolonged reaction time facilitate the formation of more stable LiLuF₄ crystals. The substitution of PEG for NH₄HF₂ changes the morphology of the product, as shown by the appearance of crystal facets (101) and (112) in the PEG-assisted crystals. The average size of the crystals can be controlled by the concentration of precursors in an aqueous solution. We demonstrate solid-state laser refrigeration of the Yb:LLF crystals using a focused near-infrared laser excitation source ($\lambda = 1020$ nm). A calibrated ratiometric Boltzmann analysis of the Yb³⁺ luminescence reveals laser cooling in air by more than 15 K below room temperature and in water by more than 5 K below room temperature.

Supplementary Materials: The following supporting information can be downloaded at: <https://www.mdpi.com/article/10.3390/app12020774/s1>, Figure S1: Scanning electron microscope images of crystals following PEG-assisted hydrothermal synthesis at: (a) 100 °C (scale bar is 1 μ m), (b) 120 °C (scale bar is 1 μ m), (c) 130 °C (scale bar is 1 μ m), (d) 180 °C (scale bar is 2 μ m), (e) 200 °C (scale bar is 2 μ m) and (f) 220 °C (scale bar is 5 μ m), for 24 h, Figure S2: Powder XRD pattern of crystals following PEG-assisted hydrothermal synthesis at 130 °C for: (a) 3 h, (b) 5 h, (c) 14 h, (d) 24 h, Figure S3: Scanning electron microscope images of crystals following PEG-assisted hydrothermal synthesis at 130 °C for: (a) 3 h (scale bar is 1 μ m), (b) 5 h (500 nm), (c) 14 h (1 μ m), (d) 24 h (1 μ m), Figure S4: Temperature-calibrated PL spectra of Yb³⁺:LLF, Figure S5: ATR-FTIR spectra of Yb³⁺:LLF synthesized under following conditions: (a) at 130 °C for 14 h; (b) at 150 °C for 5 h; (c) at 200 °C for 24 h; (d) at 200 °C for 72 h; (e) at 220 °C for 5 h; (f) at 220 °C for 48 h, Figure S6: Powder XRD pattern of crystals following PEG-assisted hydrothermal synthesis at 220 °C for 2 h (a) without calcination and calcination at: (b) 300 °C, (c) 500 °C, (d) 600 °C, Figure S7: Scanning electron microscope images of crystals following PEG-assisted hydrothermal synthesis at 220 °C for 2 h (a) without calcination and calcination at: (b) 300 °C, (c) 500 °C h, (d) 600 °C. Scale bar is 1 μ m, Figure S8: Scanning electron microscope images of LLF crystals following PEG-assisted hydrothermal synthesis at 200 °C for 24 h. (a) RE nitrate precursor amount is 4 mmol. Scale bar is 5 μ m. (b) RE nitrate precursor amount is 16 mmol. Scale bar is 20 μ m.

Author Contributions: Conceptualization, E.A.D. and P.J.P.; methodology, E.A.D. and P.J.P.; software, E.A.D., A.P. and X.X.; validation, R.E.G.; formal analysis, E.A.D., A.P. and X.X.; investigation, E.A.D., A.P., X.X. and R.E.G.; resources, P.J.P.; data curation, E.A.D., X.X., A.P. and R.E.G.; writing—original draft preparation, E.A.D.; writing—review and editing, E.A.D., A.P., X.X., R.E.G. and P.J.P.; visualization, E.A.D., A.P. and X.X.; supervision, E.A.D. and P.J.P.; project administration, E.A.D. and P.J.P.; funding acquisition, P.J.P. All authors have read and agreed to the published version of the manuscript.

Funding: E.A.D., R.E.G. and P.J.P. acknowledge support from the National Science Foundation through the UW Molecular Engineering Materials Center, a Materials Research Science and Engineering Center (DMR-1719797). A.P., X.X. and P.J.P. acknowledge financial support from the MURI:MARBLE project under the auspices of the Air Force Office of Scientific Research (Award No. FA9550-16-1-0362). Part of this work was conducted at the Molecular Analysis Facility, a National Nanotechnology Coordinated Infrastructure site at the University of Washington, which is supported in part by the National Science Foundation (grant ECC-1542101).

Institutional Review Board Statement: Not applicable.

Informed Consent Statement: Not applicable.

Data Availability Statement: The data presented in this study are available on request from the corresponding author.

Acknowledgments: We acknowledge Mikhail Kosobokov (N.D. Zelinsky Institute of Organic Chemistry of the Russian Academy of Sciences) for his useful recommendations for hydrothermal synthesis of the Yb:LLF crystals.

Conflicts of Interest: The authors declare no conflict of interest.

References

1. Skripka, A.; Karabanovas, V.; Jarockyte, G.; Marin, R.; Tam, V.; Cerruti, M.; Rotomskis, R.; Vetrone, F. Decoupling theranostics with rare earth doped nanoparticles. *Adv. Funct. Mater.* **2019**, *29*, 1807105. [[CrossRef](#)]
2. Huang, P.; Zheng, W.; Zhou, S.; Tu, D.; Chen, Z.; Zhu, H.; Li, R.; Ma, E.; Huang, M.; Chen, X. Lanthanide-doped LiLuF₄ upconversion nanoprobe for the detection of disease biomarkers. *Angew. Chem. Int. Ed.* **2014**, *53*, 1252–1257. [[CrossRef](#)] [[PubMed](#)]
3. Qin, Q.-S.; Zhang, P.-Z.; Sun, L.-D.; Shi, S.; Chen, N.-X.; Dong, H.; Zheng, X.-Y.; Li, L.-M.; Yan, C.-H. Ultralow-power near-infrared excited neodymium-doped nanoparticles for long-term in vivo bioimaging. *Nanoscale* **2017**, *9*, 4660–4664. [[CrossRef](#)] [[PubMed](#)]
4. Tsuboi, T.; Shimamura, K. Temperature sensitive near-infrared luminescence of Er³⁺ ions in LiYF₄. *Phys. Status Solidi C* **2011**, *8*, 2833–2836. [[CrossRef](#)]
5. Skripka, A.; Morinvil, A.; Matulionyte, M.; Cheng, T.; Vetrone, F. Advancing neodymium single-band nanothermometry. *Nanoscale* **2019**, *11*, 11322–11330. [[CrossRef](#)]
6. Meijer, M.S.; Rojas-Gutierrez, P.A.; Busko, D.; Howard, I.A.; Frenzel, F.; Würth, C.; Resch-Genger, U.; Richards, B.S.; Turshatov, A.; Capobianco, J.A.; et al. Absolute upconversion quantum yields of blue-emitting LiYF₄:Yb³⁺, Tm³⁺ upconverting nanoparticles. *Phys. Chem. Chem. Phys.* **2018**, *20*, 22556–22562. [[CrossRef](#)] [[PubMed](#)]
7. Huang, P.; Zheng, W.; Tu, D.; Shang, X.; Zhang, M.; Li, R.; Xu, J.; Liu, Y.; Chen, X. Unraveling the electronic structures of neodymium in LiLuF₄ nanocrystals for ratiometric temperature sensing. *Adv. Sci.* **2019**, *6*, 1802282. [[CrossRef](#)] [[PubMed](#)]
8. Shin, J.; Kyhm, J.-H.; Hong, A.-R.; Song, J.D.; Lee, K.; Ko, H.; Jang, H.S. Multicolor tunable upconversion luminescence from sensitized seed-mediated grown LiGdF₄:Yb, Tm-based core/triple-shell nanophosphors for transparent displays. *Chem. Mater.* **2018**, *30*, 8457–8464. [[CrossRef](#)]
9. Kim, S.Y.; Won, Y.-H.; Jang, H.S. A strategy to enhance Eu³⁺ emission from LiYF₄:Eu nanophosphors and green-to-orange multicolor tunable, transparent nanophosphor-polymer composites. *Sci. Rep.* **2015**, *5*, 7866. [[CrossRef](#)]
10. Gao, W.; Wang, R.; Han, Q.; Dong, J.; Yan, L.; Zheng, H. Tuning red upconversion emission in single LiYF₄:Yb³⁺/Ho³⁺ microparticle. *J. Phys. Chem. C* **2015**, *119*, 2349–2355. [[CrossRef](#)]
11. Cheng, T.; Marin, R.; Skripka, A.; Vetrone, F. Small and bright lithium-based upconverting nanoparticles. *J. Am. Chem. Soc.* **2018**, *140*, 12890–12899. [[CrossRef](#)]
12. Chen, X.; Xu, W.; Song, H.; Chen, C.; Xia, H.; Zhu, Y.; Zhou, D.; Cui, S.; Dai, Q.; Zhang, J. Highly efficient LiYF₄:Yb³⁺, Er³⁺ upconversion single crystal under solar cell spectrum excitation and photovoltaic application. *ACS Appl. Mater. Interfaces* **2016**, *8*, 9071–9079. [[CrossRef](#)]
13. Mahalingam, V.; Naccache, R.; Vetrone, F.; Capobianco, J.A. Sensitized Ce³⁺ and Gd³⁺ ultraviolet emissions by Tm³⁺ in colloidal LiYF₄ nanocrystals. *Chem.—A Eur. J.* **2009**, *15*, 9660–9663. [[CrossRef](#)] [[PubMed](#)]
14. Seletskiy, D.V.; Melgaard, S.D.; Bigotta, S.; Di Lieto, A.; Tonelli, M.; Sheik-Bahae, M. Laser cooling of solids to cryogenic temperatures. *Nat. Photonics* **2010**, *4*, 161. [[CrossRef](#)]
15. Melgaard, S.D.; Seletskiy, D.V.; Di Lieto, A.; Tonelli, M.; Sheik-Bahae, M. Optical refrigeration to 119 K, below national institute of standards and technology cryogenic temperature. *Opt. Lett.* **2013**, *38*, 1588. [[CrossRef](#)] [[PubMed](#)]
16. Rahman, A.A.; Barker, P. Laser refrigeration, alignment and rotation of levitated Yb³⁺:YLF nanocrystals. *Nat. Photonics* **2017**, *11*, 634. [[CrossRef](#)]
17. Roder, P.B.; Smith, B.E.; Zhou, X.; Crane, M.J.; Pauzauskie, P.J. Laser refrigeration of hydrothermal nanocrystals in physiological media. *Proc. Natl. Acad. Sci. USA* **2015**, *112*, 15024–15029. [[CrossRef](#)]

18. Xia, X.; Pant, A.; Davis, E.J.; Pauzauskie, P.J. Design of a radiation-balanced fiber laser via optically active composite cladding materials. *J. Opt. Soc. Am. B* **2019**, *36*, 3307–3314. [[CrossRef](#)]
19. Pant, A.; Xia, X.; Davis, E.J.; Pauzauskie, P.J. Solid-state laser refrigeration of a composite semiconductor Yb:YLiF₄ optomechanical resonator. *Nat. Commun.* **2020**, *11*, 3235. [[CrossRef](#)] [[PubMed](#)]
20. Xia, X.; Pant, A.; Ganas, A.S.; Jelezko, F.; Pauzauskie, P.J. Quantum point defects for solid-state laser refrigeration. *Adv. Mater.* **2021**, *33*, 1905406. [[CrossRef](#)]
21. Yasyukevich, A.S.; Mandrik, A.V.; Kuleshov, N.V.; Gordeev, E.Y.; Korableva, S.L.; Naumov, A.K.; Semashko, V.V.; Popov, P.A. Spectral kinetic properties of Yb³⁺:Na₄Y₆F₂₂ and Yb³⁺:LiLuF₄ crystals. *J. Appl. Spectrosc.* **2007**, *74*, 844–850. [[CrossRef](#)]
22. Zhou, X.; Smith, B.E.; Roder, P.B.; Pauzauskie, P.J. Laser refrigeration of ytterbium-doped sodium–yttrium–fluoride nanowires. *Adv. Mater.* **2016**, *28*, 8658–8662. [[CrossRef](#)]
23. Xia, X.; Pant, A.; Zhou, X.; Dobretsova, E.A.; Bard, A.B.; Lim, M.B.; Roh, J.Y.D.; Gamelin, D.R.; Pauzauskie, P.J. Hydrothermal synthesis and solid-state laser refrigeration of ytterbium-doped potassium-lutetium-fluoride (KLF) microcrystals. *Chem. Mater.* **2021**, *33*, 4417–4424. [[CrossRef](#)]
24. Dobretsova, E.A.; Xia, X.; Pant, A.; Lim, M.B.; De Siena, M.C.; Boldyrev, K.N.; Molchanova, A.D.; Novikova, N.N.; Klimin, S.A.; Popova, M.N. Hydrothermal synthesis of Yb³⁺: LuLiF₄ microcrystals and laser refrigeration of Yb³⁺: LuLiF₄/silicon-nitride composite nanostructures. *Laser Photonics Rev.* **2021**, *15*, 2100019. [[CrossRef](#)]
25. Zhang, Q.; Yan, B. Hydrothermal synthesis and characterization of LiREF₄ (RE = Y, Tb–Lu) nanocrystals and their core–shell nanostructures. *Inorg. Chem.* **2010**, *49*, 6834–6839. [[CrossRef](#)] [[PubMed](#)]
26. Lu, C.; Huang, W.; Ni, Y.; Xu, Z. Hydrothermal synthesis and luminescence properties of octahedral LiYbF₄:Er³⁺ microcrystals. *Mater. Res. Bull.* **2011**, *46*, 216–221. [[CrossRef](#)]
27. Huang, W.; Lu, C.; Jiang, C.; Jin, J.; Ding, M.; Ni, Y.; Xu, Z. Rare earth doped LiYbF₄ phosphors with controlled morphologies: Hydrothermal synthesis and luminescent properties. *Mater. Res. Bull.* **2012**, *47*, 1310–1315. [[CrossRef](#)]
28. Luo, R.; Li, T.; Chen, Y.; Ning, Z.; Zhao, Y.; Liu, M.; Lai, X.; Zhong, C.; Wang, C.; Bi, J.; et al. Na_(1-x)Li_x(Gd_{0.39}Y_{0.39}Yb_{0.2}Er_{0.02})f₄ (0 ≤ x ≤ 1) solid solution microcrystals: Li/Na ratio-induced transition of crystalline phase and morphology and their enhanced upconversion emission. *Cryst. Growth Des.* **2018**, *18*, 6581–6590. [[CrossRef](#)]
29. Littleford, T.E.; Jackson, R.A.; Read, M.S.D. An atomistic simulation study of the effect of dopants on the morphology of YLiF₄. *Phys. Status Solidi C* **2013**, *10*, 156–159. [[CrossRef](#)]
30. Littleford, T.E.; Jackson, R.A.; Read, M.S. An atomistic surface simulation study predicting morphologies and segregation in yttrium lithium fluoride. *Surf. Sci.* **2012**, *606*, 1550–1555. [[CrossRef](#)]
31. Azzurra, V.; Giovanni, C.; Alberto Di, L.; Arlete, C.; Hans, P.J.; Mauro, T. Investigation of yb-doped LiLuF₄ single crystals for optical cooling. *Opt. Eng.* **2016**, *56*, 1–5.
32. Fedorov, P.P.; Aleksandrov, V.B.; Bondareva, O.S.; Buchinskaya, I.I.; Val’Kovskii, M.D.; Sobolev, B.P. Concentration dependences of the unit-cell parameters of nonstoichiometric fluorite-type Na_{0.5-x}R_{0.5+x}F_{2+2x} phases (R = rare-earth elements). *Crystallogr. Rep.* **2001**, *46*, 239–245. [[CrossRef](#)]